Contents lists available at ScienceDirect

Nuclear Instruments and Methods in Physics Research B

Electrical properties of silicon diodes with p+n junctions irradiated with ^{197}Au^{+26} swift heavy ions

N.A. Poklonski [a,*], N.I. Gorbachuk [a], S.V. Shpakovski [b], A.V. Petrov [c], S.B. Lastovskii [c], D. Fink [d], A. Wieck [e]

[a] Department of Physics, Belarusian State University, pr. Nezavisimosti 4, BY-220030 Minsk, Belarus
[b] "Transistor Plant" Unitary Enterprise of the SPE "Integral", ul. Korzhenevskogo 108, BY-220064 Minsk, Belarus
[c] Scientific-Practical Materials Research Centre NAS of Belarus, ul. P. Brovki 19, BY-220072 Minsk, Belarus
[d] Hahn-Meitner-Institute, 100 Glienicker Strasse, D-14109 Berlin, Germany
[e] Ruhr-Universitaet Bochum, 150 Universitaetsstrasse, D-44780 Bochum, Germany

ARTICLE INFO

ABSTRACT

Electrical properties of silicon diodes with p+n junctions irradiated with ^{197}Au^{+26} swift heavy ions (energy $E = 350$ MeV, fluences of 10^7 cm^{-2} and 10^8 cm^{-2}) and silicon diodes irradiated with electrons (energy $E = 3.5$ MeV, fluences of 10^{15} cm^{-2}, 5×10^{15} cm^{-2} and 10^{16} cm^{-2}) have been investigated. Frequency dependences of the impedance, current–voltage characteristics and switching characteristics of these devices have been studied. Irradiation of the diodes with ^{197}Au^{+26} ions at a fluence of 10^8 cm^{-2} leads to the formation of a quasi-continuous layer of irradiation-induced defects that enable a combination of characteristics such as a reverse resistance recovery time and direct voltage drop that are better than those for electron-irradiated diodes. Still, the irradiation of high-energy ions results in an increase in recombination currents that are larger than those obtained with electron irradiation, and causes more complicated frequency dispersion of the diode parameters.

1. Introduction

As a rule, doping with gold (and more rarely, with platinum) is used in the manufacturing of impulse and quick-response silicon diodes and transistors to decrease the lifetime of non-equilibrium charge carriers [1]. Alternatively, electron irradiation (or, more rarely, irradiation with gammas, protons and alpha rays) is used for this purpose [1–3]. For irradiation with electrons and gammas, irradiation-induced defects are created uniformly in the volume of the semiconductor. Irradiation with protons [4] or alpha rays [5–8] enables the formation of layers with increasing irradiation-induced defects content, and the width of these layers is smaller than the base thickness (sometimes to a great extent). Stepwise irradiation treatment of a material with electrons and protons (or alpha rays) makes it possible to control the irradiation-induced defect distribution profile [9–11]. This processing technology leads to good

results in the formation of quick-response diodes with a slow recovery of reverse resistance [3,8,10–12].

It is also well known that irradiation with swift heavy ions leads to the formation of high concentrations of point defects along the swift heavy ion track (along with a creation of amorphous areas) [13,14]. High-energy ion implantation has been used for the creation of instrumental structures on the basis of high bandgap semiconductors [15,16] and improvement of the properties of barrier structures on silicon [17]. For instance, in [16] the concept of a transistor based on a single ion track has been suggested, and the authors of [17] have used silver ion implantation to control a potential barrier in a Au/n-Si Schottky diode.

A high concentration of point defects in the areas of their agglomeration and the use of impurity ions (for instance, gold ones) to introduce deep levels in the bandgap would be useful to create areas of specific geometry with increased recombination rates. These structures would allow for the creation of diodes with a fast switching speed. Also, if the thickness of the layer that has been transformed by ion implantation is small, it can enable

* Corresponding author. Tel.: +375 172095110; fax: +375 172095445.
  E-mail addresses: poklonski@bsu.by, poklonski@tut.by (N.A. Poklonski).

minimal values of direct voltage drop. This is important for decreasing power dissipation.

The aim of the present work is to investigate the electrical properties of diodes irradiated with ^{197}Au^{+26} swift heavy ions and to compare them to the properties of diodes irradiated with electrons.

2. Experimental technique

The diodes were made on wafers of n-type single-crystalline silicon uniformly doped with P. The resistivity of the wafers ((1 1 1) plate, thickness 460 μm) was 90 Ω cm. An anodic area of p-type was created by B$^+$ ion implantation (p$^+$n junction occurrence depth $x_j \approx 13$ μm). P$^+$ ion implantation in the non-planar side of the wafer ($E = 75$ keV, radiation dose 500 μC/cm^2) was carried out for the creation of an Ohmic contact to the diode base. Electrical contacts were formed by Al sputtering with their subsequent burning-in at 475 °C in nitrogen atmosphere.

The diodes were irradiated with ^{197}Au^{+26} swift heavy ions at the "ISL" accelerator center of the Hahn–Meitner–Institute (Berlin, Germany). The energy of the irradiation was 350 MeV, the fluxes were always kept well below 1 nA to avoid sample heating, and the fluences were 10^7 cm^{-2} and 10^8 cm^{-2}. The irradiation was performed on the planar side of the diodes perpendicular to the p$^+$n junction plane.

The diodes were irradiated with 3.5 MeV electrons at a fluence (Φ) of 10^{15} cm^{-2} in pulse mode at room temperature at the Scientific-Practical Materials Research Centre NAS of Belarus (Minsk, Belarus). The value of the fluence of electron irradiation was selected to assure that the reverse resistance recovery time is comparable in magnitude to the value for diodes irradiated with ^{197}Au^{+26} ions.

Both the real and imaginary parts of the impedance Z of the diodes were measured at a frequency range of 20 Hz–1 MHz on an Agilent 4284A LCR-meter. The bias voltage was varied from +0.2 V to −10 V. The measurements were carried out at the Ruhr-Universitaet Bochum (Germany).

The static current–voltage characteristics were measured by a standard technique on an HP 4156B setup. The reverse resistance recovery time of the diodes was investigated with the UNIPRO measuring setup by the injection–extraction method [18]. All of the measurements were carried out at room temperature. DLTS spectra of the diodes were registered in the 80−330 K temperature range.

3. Experimental results and discussion

The switching characteristics are presented in Fig. 1 for initial diodes (dependence 1), diodes irradiated with ^{197}Au^{+26} ions at $\Phi = 10^7$ cm^{-2} (dependence 4), $\Phi = 10^8$ cm^{-2} (dependence 2) and diodes irradiated with electrons at $\Phi = 10^{15}$ cm^{-2} (dependence 3). Irradiation with ^{197}Au^{+26} at 10^8 cm^{-2} leads to a comparable decrease of reverse resistance recovery time as irradiation with electrons at a fluence of 10^{15} cm^{-2}.

Current–voltage characteristics are given in Fig. 2 for initial diodes (dependence 1), diodes irradiated with gold ions at $\Phi = 10^8$ cm^{-2} (dependence 2) and diodes irradiated with electrons at $\Phi = 10^{15}$ cm^{-2} (dependence 3). It follows from the comparison of transition characteristics given in Fig. 1 that irradiation with ^{197}Au^{+26} leads to an increase of the diode base resistance. Nevertheless, this increase is considerably lower than that in the case of electron irradiation. At the same time, recombination currents in diodes irradiated with gold ions are larger by several orders of magnitude.

It should be noted that there is a considerable difference in the switching characteristics of the diodes irradiated with gold ions at
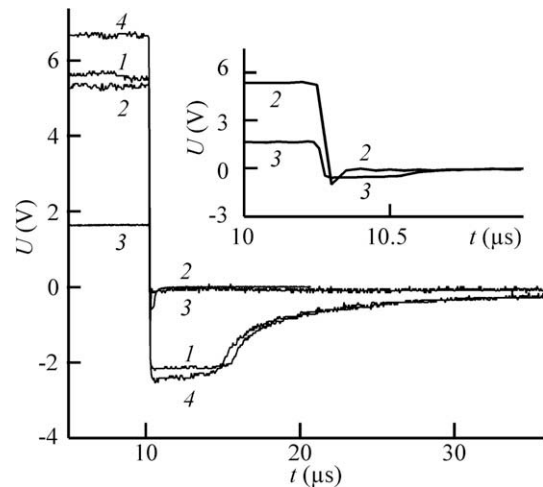

Fig. 1. Switching characteristics of diodes: initial (1), irradiated with ^{197}Au^{+26} ions at $\Phi = 10^8$ cm^{-2} (2) and $\Phi = 10^7$ cm^{-2} (4), and irradiated with electrons at $\Phi = 10^{15}$ cm^{-2} (3).
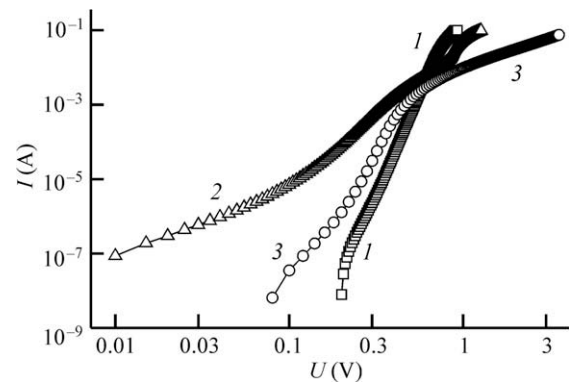

Fig. 2. Current–voltage characteristics of diodes: initial (1), irradiated with ^{197}Au^{+26} ions at $\Phi = 10^8$ cm^{-2} (2), and irradiated with electrons at $\Phi = 10^{15}$ cm^{-2} (3).

fluences of 10^7 cm^{-2} and 10^8 cm^{-2}. As shown in Fig. 1, the fluence increase from 10^7 cm^{-2} to 10^8 cm^{-2} (by an order of magnitude) leads to a decrease of the reverse resistance recovery time from $\tau_r \approx 8$ μs to $\tau_r \approx 50$ ns (i.e. by larger than two orders of magnitude). The reasons for such sharp changes in the diode parameters are discussed below.

The areas of irradiation-induced aggregates of defects [19,20] and, in some cases, tracks (see details in [13]) appear in the silicon during the swift ion passage. The formation of new types of lattice defects with a fluence increase from 10^7 cm^{-2} to 10^8 cm^{-2} is unlikely [13]. Thus, considerable change in the reverse resistance recovery time τ_r may be associated with the features of defect distribution over the depth or over the plane of the diode structure. According to calculations carried out by the TRIM program (see Fig. 3), the maximum of the primary vacancy distribution profile on the diode depth is observed at ≈23 μm. There are no principle distinctions in the distribution of the irradiation-induced defects over the depth of the structure at fluences of 10^7 cm^{-2} and 10^8 cm^{-2} [19].

Let us consider the effect of the presence of the irradiation-induced defect aggregates on the recombination of non-equilibrium holes during their diffusion into the base. The relaxation of the injected holes takes place due to their diffusion [18] if the electric field between the space–charge area and the base as well as the fields between the areas of irradiation-induced defects and the undamaged regions of the base are ignored. The holes that diffuse
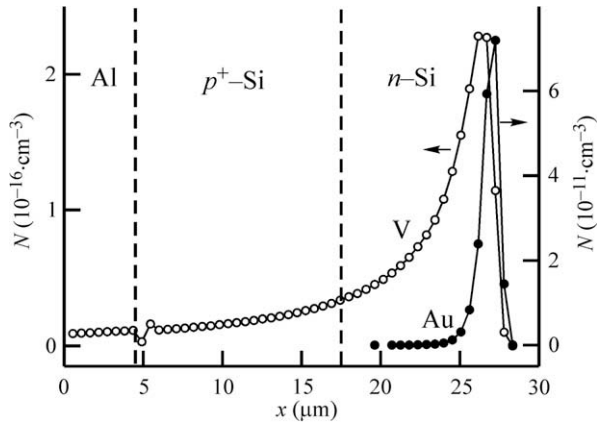
Fig. 3. Calculated distribution profiles of implanted $^{197}\text{Au}^{+26}$ ions (dark circles) and primary vacancies (V) at $\Phi = 10^8\ \text{cm}^{-2}$.

deep into the base are trapped and recombine with the irradiation-induced defects. The recombination rate (i.e. the number of the recombining holes per unit time in a unit volume) in the area of irradiation-induced defects formed by the passage of a single $^{197}\text{Au}^{+26}$ ion depends on the type and local concentration of the irradiation-induced defects and the position of the quasi-Fermi level [18]. The recombination rate does not depend on the irradiation fluence until the irradiation-induced areas are overlapped. The recombination rate of the injected holes recalculated for the whole volume of the base (i.e. the recombination effectiveness) is proportional to the 'volume' of the irradiation-induced defect aggregates. A considerable increase in the hole recombination effectiveness should be expected when the areas of the irradiation-induced defect aggregates start to merge. Let us estimate the possibility of the formation of a quasi-continuous layer of irradiation-induced defects by comparing the consequences of the irradiation with fluences of $10^7\ \text{cm}^{-2}$ and $10^8\ \text{cm}^{-2}$.

The passage of the ion in the crystal leads to the development of secondary recoil cascades [13,19,20]. As an example, Fig. 4 shows a calculation of the primary vacancies created as a result of the passage of a single $^{197}\text{Au}^{+26}$ ion with energy 350 MeV, performed using
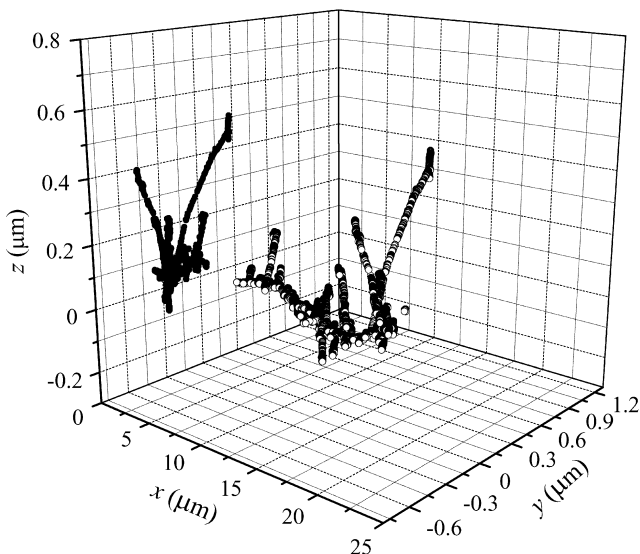
the TRIM program. The point defects created in the secondary cascades migrate and 'fill intervals' between them, resulting in the formation of the area of the irradiation-induced defect aggregate. Let us consider for simplicity that the irradiation-induced defect aggregate area is axially symmetric and does not possess internal structure (e.g. a track type structure in which a multi-vacancy nuclear is surrounded with a shell enriched with interstitial atoms [13]). The area s of the projection of this heavily damaged region on the plane of the p^+n junction is a random quantity. For the estimate of s, the following quantity was used

$$R_{V\perp} = \frac{1}{N} \sum_{i=1}^{N} \sqrt{(Y_V)_i^2 + (z_V)_i^2}, \tag{1}$$

where $(y_V)_i$, $(z_V)_i$ are the coordinates of the primary vacancies, and N is the number of vacancies after the passage of an $^{197}\text{Au}^{+26}$ ion. The x axis is perpendicular to the plane of the p^+n junction and is oriented in the direction of implantation. The point of ion entry into the target was chosen as the origin of coordinates. In this case, $R_{V\perp}$ is the average (within a single damaged region) deviation of the projections of the lattice sites 'occupied' with vacancies on the plane perpendicular to the implantation direction. The average value of $R_{V\perp}$ (over the total implanted into diode $^{197}\text{Au}^{+26}$ ions) was taken to improve the estimate [21],

$$\langle R_{V\perp} \rangle = \frac{1}{\Phi A} \sum_{k=1}^{\Phi A} (R_{V\perp})_k, \tag{2}$$

where A is the area of the p^+n junction. The average value of s is approximately equal to $\langle s \rangle \approx \pi \cdot \langle R_{V\perp} \rangle^2$. The total area S of the projections of the irradiation-induced defect aggregates is estimated as $S = A\Phi \langle s \rangle$. If $\Phi[\text{cm}^{-2}]\ \langle s \rangle[\text{cm}^2] \approx 1$, it is likely that a layer of quasi-continuous irradiation-induced defects is formed.

The calculations of $R_{V\perp}$ using Eq. (1) were performed on the basis of the results of the simulation in the TRIM program for 100 instances of the passage of a single $^{197}\text{Au}^{+26}$ ion with energy 350 MeV. The average value calculated using Eq. (2) is $\langle R_{V\perp} \rangle \approx 0.53\ \mu\text{m}$. Thus, the creation of the irradiation-induced defect aggregate with $\langle s \rangle \approx \pi \cdot \langle R_{V\perp} \rangle^2 \approx 0.88\ \mu\text{m}^2 = 0.88 \times 10^{-8}\ \text{cm}^2$ may be attributed to a single ion passage. We obtain the value $\Phi \cdot \langle s \rangle \approx 0.88$, which is close to 1 at the fluence of $10^8\ \text{cm}^{-2}$. This allows us to rely on the formation of the 'quasi-continuous' layer of the irradiation-induced defects for the non-equilibrium charge carriers (holes) diffusing into the base. For the fluence of $10^7\ \text{cm}^{-2}$, the value $\langle s \rangle \cdot \Phi$ is smaller by an order of magnitude. Consequently, only the isolated regions of irradiation-induced defect aggregates can be considered in this case. Note that the detailed consideration of the non-equilibrium charge carriers would lead only to the increase of the $\langle s \rangle$ estimate due to the necessity of taking into account the hole distribution in the plane of the base (non-homogeneous in the case of the isolated regions).

It follows from the obtained data that a layer with increased recombination rates formed by the $^{197}\text{Au}^{+26}$ ion implantation makes it possible not only to obtain the same small value of a diode's reverse resistance recovery (see Fig. 1) as after electron irradiation at $\Phi = 10^{15}\ \text{cm}^{-2}$, but also to obtain at the same time a considerably smaller diode base resistance (see Fig. 2). This is connected with the fact that for the case of 3.5 MeV electron irradiation, the defects are introduced throughout the entire diode depth leading to an increase of resistivity of the whole diode base. For the case of irradiation with 350 MeV $^{197}\text{Au}^{+26}$ ions, the maximum of the irradiation-induced defects and Au impurities is concentrated at the depth 15–25 μm (relative to the silicon surface). At depth values larger than 30 μm (see Fig. 3), the diode base is practically free from defects and keeps the initial resistivity value. Due to the small thickness of the recombination layer, the general growth of the base resistance is considerably smaller than for the

Fig. 4. Calculated distribution (over the space) of the primary vacancies created in the silicon by the implantation of an $^{197}\text{Au}^{+26}$ ion (light circles) and their projections on the plane perpendicular to the implantation direction (dark circles). Vacancies in the aluminium layer and p^+-Si are not shown.

case of electron irradiation. Still, comparing to electron irradiation, the implantation of high-energy ions causes formation of irradiation-induced defects with significant concentration in the space–charge region, leading to larger recombination currents (Fig. 2).

The presence of the layer with high-resistance and consequently large dielectric (Maxwell) relaxation time transforms the base of the diode into a heterogeneous system. The importance of the problem of the Maxwell relaxation time increase in the irradiated silicon is noted in previous works [22,23]. According to [24], the complicated dependence of the impedance Z on the alternating current frequency f is typical for heterogeneous systems.

Dependences of the imaginary part of the impedance Z'' on the AC frequency f in the absence of a bias voltage are given in Fig. 5, normalized to a maximum value Z''_m. The curve enumeration corresponds to that given in Fig. 2. It should be noted that for an implantation fluence of $\Phi = 10^7$ cm^{-2}, the changes in $Z''(f)$ are not significant. Two peaks can be distinguished in the $Z''(f)$ dependences for the diode irradiated with ^{197}Au^{+26} ions ($\Phi = 10^8$ cm^{-2}). The first one is in the vicinity of 5 kHz. Its position corresponds to the condition $\omega\tau_{pn} = 1$ [25], where $\tau_{pn} = RC$ is a time constant of the p$^+$n junction and $\omega = 2\pi f$ is a cyclic frequency. The peak is shifted to larger frequencies when compared to the $Z''(f)$ dependences for initial diodes and for electron-irradiated diodes (see Fig. 5(a)). This can be explained by a decrease of space–charge layer resistivity by means of intensification of charge carrier generation and recombination processes on irradiation-induced defects. A second peak in the $Z''(f)$ dependence, f_m, is placed in the vicinity of about 100 kHz (see Fig. 5(a)), and, correspondingly, it is characterized by the time constant $\tau_\delta \approx 10^{-6}$ s. The impedance plot of the

diode irradiated with ^{197}Au^{+26} ions (see inset in Fig. 5(b)) is actually a sum of two 'semicircles'.

The equivalent circuit consisting of two serially connected RC circuits is considered during investigation of the frequency dependences of the diodes with the high-resistance base: neutron irradiated pin diodes [26] and diodes on the basis of the silicon carbide [27]. One of the RC circuits corresponds to the space–charge area and the other to the high-resistance base. It is known that the impedance plot of such an equivalent circuit, for the considerably different time constants of the RC circuits, is a sum of two semicircles [24], and in the frequency dependences of the imaginary part of the impedance, the two peaks can be observed. The experimental results shown in Fig. 5 correspond to these concepts, taking into account that in our case the increased values of resistance do not refer to the whole base but only to the thin damaged layer. Employing different equivalent circuits (with the same number of resistors and capacitors) [24] giving identical frequency dependences of the impedance is impractical due to the complications associated with establishing the correspondence between the circuit elements and the 'structural components' of the diode.

It is known [28] that with the increase of the irradiation-induced defects, the electrical conductivity of the silicon approaches the conductivity of the intrinsic crystal. The resistivity ρ of the silicon with the irradiation-induced structural defects considered in [28] was $\rho \approx 10^5 \, \Omega$ cm at a temperature of 300 K. The value $\rho \approx 3.16 \times 10^5 \, \Omega$ cm for the intrinsic silicon is given in the handbook [29]. These data allow us to estimate the Maxwell relaxation time τ_M in the heavily damaged layer as $\tau_M = \varepsilon\varepsilon_0\rho = (1-3.3) \times 10^{-7}$ s, where $\varepsilon = 11.7$ is the permittivity of the silicon, ε_0 is the electric constant, and the resistivity is close to the intrinsic silicon resistivity. Thus, the position of the corresponding maximum in the dependence of the imaginary part of the impedance Z'' on the frequency f of the alternating current is $f_m = 1/(2\pi\tau_M) = 1.5-0.5$ MHz. This estimate gives an approximately 5 times larger value of f_m than observed in our experiment (see curve 2 in Fig. 5(a)). Nevertheless, since the permittivity ε of the silicon with irradiation-induced defects can increase by an order of magnitude [30,31], the second peak in the $Z''(f)$ dependence (and the second semicircle in the impedance plot) for the diodes irradiated with gold may be accounted for by the presence of the irradiation damaged silicon layer.

An alternative explanation of the mentioned features of the frequency dependences of the diodes irradiated with ^{197}Au^{+26} ions with $\Phi = 10^8$ cm^{-2} is deep level recharging or polarisation on the interfaces between the undamaged base and the areas of the point defect aggregates formed by single ^{197}Au^{+26} ions, as considered in [1]. For this case, however, the second peak in the $Z''(f)$ (and the second semicircle in the impedance plot) should be observed for the implantation fluence of 10^7 cm^{-7}, which contradicts our experimental results. Thus, the most likely reason for the observed $Z''(f)$ dependences is the formation of the layer with an increased content of irradiation-induced defects.

The recharging process most probably manifests itself in the 'broadening' of the low-frequency (first) peak. In Fig. 6, the $Z''(f)/Z''_m$ dependences on the dimensionless frequency $2\pi f\tau_{pn}$ are shown. Dependence 1 is made for the diode irradiated with ^{197}Au^{+26} ions ($\Phi = 10^7$ cm^{-7}), and dependence 2 shows the calculated values of $Z''/Z''_m = 2\omega\tau_{pn}/(1 + (\omega\tau_{pn})^2)$, which describes a single parallel RC circuit.

A bias voltage with negative polarity leads to an increase of the p$^+$n junction resistivity and a shift of the first peak of the $Z''(f)$ dependence towards a low-frequency region. This is clearly seen in Fig. 7 where the dependences of the imaginary part of the normalized impedance Z''/Z''_m on the frequency f are shown for ^{197}Au^{+26} irradiated diodes at bias voltage values 0 (dependence 1), −0.02 V (2), −0.04 V (3), −0.1 V (4), and −0.2 V (5). Here a shift of
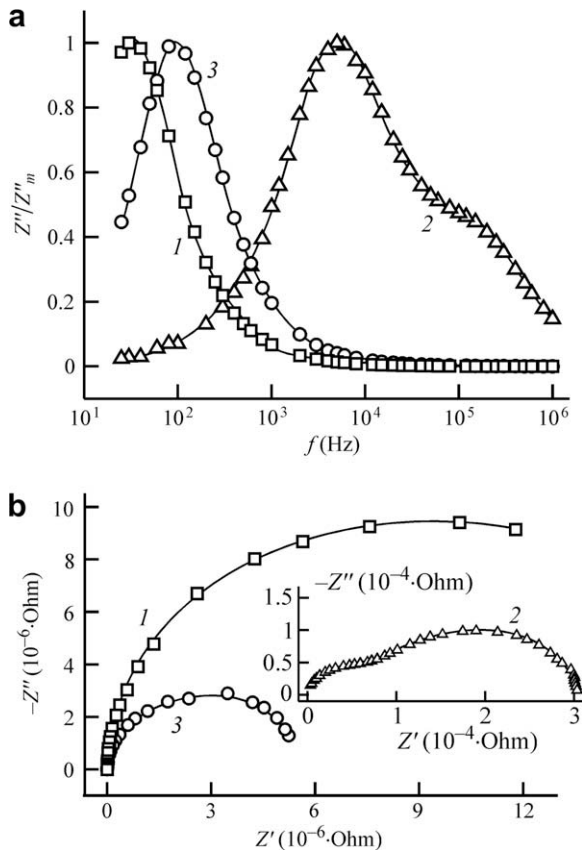

Fig. 5. Dependences of the imaginary part of the impedance Z'' on frequency f (a), and impedance plots (b): 1 is for the initial diode, 2 is for the diode irradiated with ^{197}Au^{+26} ions at $\Phi = 10^8$ cm^{-2}, and 3 is for diode irradiated with electrons at $\Phi = 10^{15}$ cm^{-2}. The dependences are normalized to the maximal value of Z''_m.
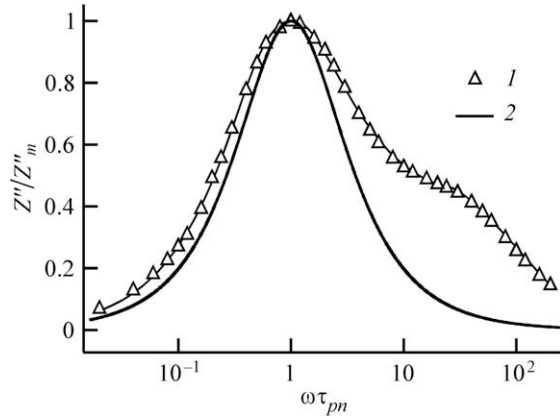
Fig. 6. Dependences of the imaginary part of the impedance (normalized to a maximal magnitude) on the dimensionless frequency $\omega\tau_{pn}$: *1* shows the experimental values for the diode irradiated with $^{197}Au^{+26}$ ions at $\Phi = 10^8$ cm^{-2} and *2* is the theoretical dependence for a parallel RC circuit.

the second peak takes place as well, and the peak from the heavily damaged silicon layer "vanishes" on its background, due to a large increase of space–charge layer resistivity.

Applying small positive polarity voltages to the diode leads to a shift of both the first and second peaks towards the high frequency area. $Z''(f)/Z''_m$ dependences at bias voltage values 0 (dependence *1*), 0.04 V (*2*), and 0.1 V (*3*) are shown in Fig. 8. A shift of the peak

Fig. 8. Dependences of the imaginary part of the impedance Z'' on frequency f (a) and impedance plots (b) at the following direct bias voltage values: 0 (dependence *1*), 0.04 V (*2*), and 0.1 V (*3*). The dependences are normalized to the maximal value Z''_m. The diode is irradiated with $^{197}Au^{+26}$ ions at $\Phi = 10^8$ cm^{-2}.

corresponding to the p$^+$n junction is caused by a decrease of the space–charge layer thickness. A change of the peak position, caused by the presence of a heavily damaged silicon layer, takes place because the charge carriers injection lowers the silicon layer resistivity.

The damaged layer includes both the irradiation-induced defects and the gold impurity itself. In Fig. 9, the DLTS spectra registered in the regimes of emission (*1*) and injection of the charges (*2*) are shown. In our experiments, we succeeded in resolving only the peak for the defect at the depth $E_c - (0.19 \pm 0.01)$ eV, which may be identified as vacancy–oxygen complex, taking into account the experimental error. An attempt to determine the activation energies of the remaining defects failed due to their large peak widths and the presence of the anomalous peaks.

It should be noted that identification of the point defects in the silicon irradiated with swift heavy ions is a rather complex
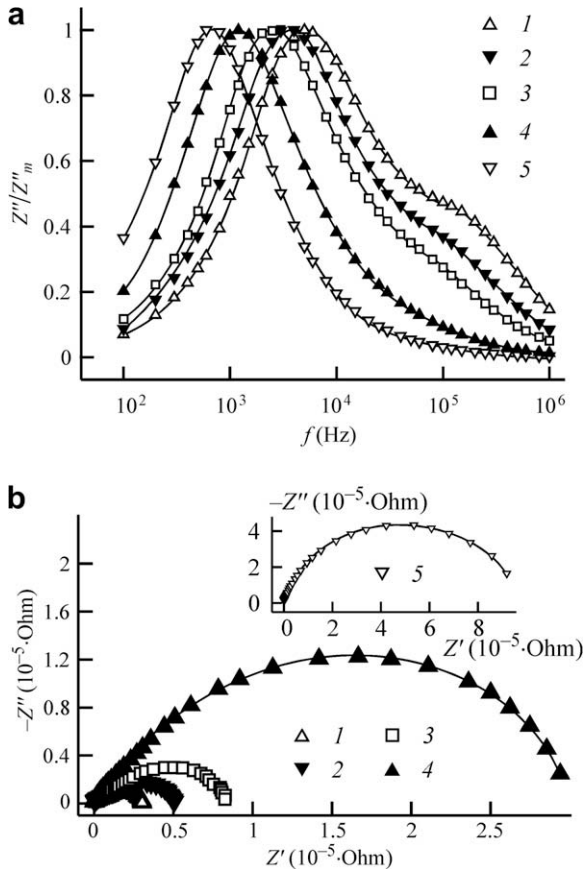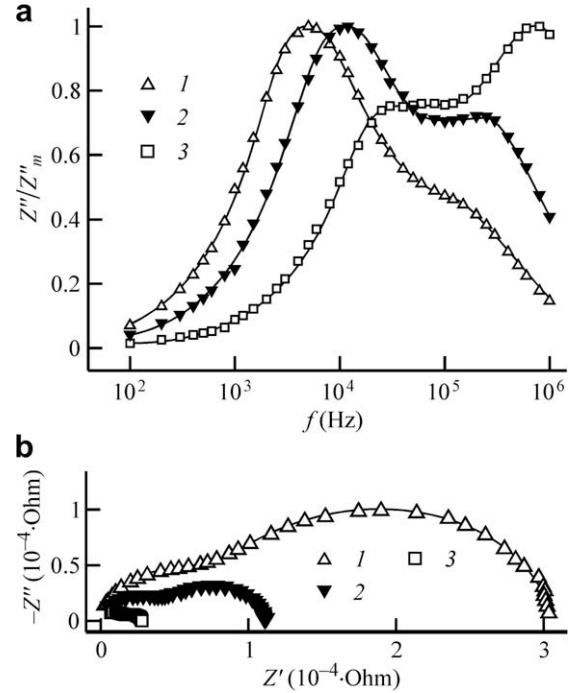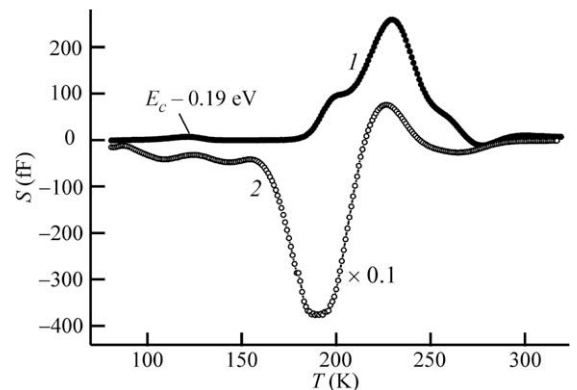

Fig. 7. Dependences of the imaginary part of the impedance Z'' on frequency f (a), and impedance plots (b) at the reverse bias voltage values 0 (dependence *1*), −0.02 V (*2*), −0.04 V (*3*), −0.1 V (*4*), and −0.2 V (*5*). The dependences are normalized to the maximal value Z''_m. The diode is irradiated with $^{197}Au^{+26}$ ions at $\Phi = 10^8$ cm^{-2}.

Fig. 9. DLTS spectra of the $^{197}Au^{+26}$ irradiated diode obtained at the charge carriers in emission mode (*1*) and injection mode (*2*).

problem (see, e.g. [32–34]) and is beyond the consideration of the present work. The formation of the divacancies, oxygen–vacancy, and carbon–oxygen complexes in concentrations ensuring their dominant role in the recombination processes can be related to the irradiation of silicon with swift heavy ions according to the results of previous work [34–38].

4. Conclusions

We conclude that the implantation of $^{197}Au^{+26}$ high-energy ions at a fluence of 10^8 cm^{-2} makes it possible to form a quasi-continuous buried layer of irradiation-induced defects with increased recombination rates, providing the same reverse resistance recovery dynamics as for diodes irradiated with electrons at a fluence of 10^8 cm^{-2}. The general resistance of the diode base (and hence the direct voltage drop) increases to a lesser degree for implantation with $^{197}Au^{+26}$ ions. Still, the $^{197}Au^{+26}$ irradiation causes a larger increase of generation–recombination currents compared to electron irradiation. This effect is primarily caused by the large concentration of irradiation-induced defects in the space–charge area and neighbouring layers of a diode base. $^{197}Au^{+26}$ implantation also leads to more changes in the frequency dependence of the diode impedance than electron-irradiated diodes or diodes containing Au impurities introduced by thermal diffusion. This considerably hinders a direct implementation of this technological method and requires carrying out further investigations. For instance, it is necessary to work out the annealing modes of irradiation-induced defects and to consider the probability of high-energy implantation with lighter ions into the non-planar side.

Acknowledgements

References

[1] A.G. Milnes, Deep Impurities in Semiconductors, Wiley, New York, 1973 (Mir, Moscow, 1977).
[2] V.S. Vavilov, B.M. Gorin, N.S. Danilin, A.E. Kiv, Yu.L. Nurov, V.I. Shakhovtsov, Radiation Methods in Solid State Electronics, Radio i Sviaz, Moscow, 1990 (in Russian).
[3] V.A. Kozlov, V.V. Kozlovskii, Semiconductors 35 (2001) 735.
[4] J.H. Kim, D.U. Lee, E.K. Kim, Y.H. Bae, Physica B 376–377 (2006) 181.
[5] A.M. Ivanov, N.B. Strokan, V.B. Shuman, Semiconductors 32 (1998) 325.
[6] A.M. Ivanov, N.B. Strokan, V.B. Shuman, Tech. Phys. Lett. 23 (1997) 369.
[7] F. Fizzoti, E. Colombo, A. Lo Giudice, C. Manfredotti, Z. Medunic, M. Jaksic, E. Vittone, Nucl. Instr. and Meth. B 260 (2007) 259.
[8] K. Nishiwaki, T. Kushida, A. Kawahashi, in: Proc. ISPSD'01 235–238, Japan, 2001.
[9] J. Vobecký, P. Hazdra, V. Záhlava, Microelectron. Reliab. 43 (2003) 537.
[10] P. Hazdra, V. Kamarnitskyy, Microelectron. J. 37 (2006) 197.
[11] P. Hazdra, J. Vobecký, H. Dorschner, K. Brand, Microelectron. J. 35 (2004) 249.
[12] S.S. Asina, V.M. Kuznetsov, A.M. Surma, T.A. Uverskaya, Elektronnaya tekhnika 1 (1985) 42 (in Russian).
[13] F.F. Komarov, Phys. Usp. 46 (2003) 1253.
[14] A.R. Chelyadinskii, F.F. Komarov, Phys. Usp. 46 (2003) 789.
[15] A.M. Zaitsev, Phys. Chem. Mech. Surf. 6, 1991, No. 10.
[16] A.M. Zaitsev, A.V. Denisenko, G. Kosaca, R. Job, W.R. Fahrner, A.A. Melnikov, V.S. Varichenko, B. Burchard, J. von Borany, M. Werner, J. Wide Bandgap Mater. 7 (1999) 4.
[17] F. Kumar, D. Kanjilal, Nucl. Instr. and Meth. B 248 (2006) 109.
[18] S.M. Sze, Semiconductor Devices: Physics and Technology, second ed., Wiley, New York, 2001.
[19] M. Nastasi, J.W. Mayer, Ion Implantation and Synthesis of Materials, Springer, Berlin, 2006.
[20] M. Nastasi, J.W. Mayer, J.K. Hirvonen, Ion–Solid Interactions. Fundamentals and Applications (Cambridge Solid State Science Series), Cambridge University Press, Cambridge, 1996.
[21] D.J. Hudson, Statistics. Lectures on Elementary Statistics and Probability, CERN, Geneva, 1964 (Mir, Moscow, 1970).
[22] M. McPherson, Nucl. Instr. and Meth. A 488 (2002) 100.
[23] M. McPherson, Physica B 344 (2004) 52.
[24] E. Barsoukov, J.R. Macdonald (Eds.), Impedance Spectroscopy: Theory, Experiment, and Applications, Wiley, Hoboken, 2005.
[25] L.S. Berman, A.A. Lebedev, Deep-level Capacitance Spectroscopy of Semiconductors, Leningrad, Nauka, 1981 (in Russian).
[26] D. Campbell, A. Chilingarov, T. Sloan, Nucl. Instr. and Meth. A 552 (2005) 152.
[27] A.A. Lebedev, A.A. Lebedev, D.V. Davydov, Semiconductors 34 (2000) 115.
[28] V.N. Brudnyi, N.G. Kolin, L.S. Smirnov, Semiconductors 41 (2007) 1011.
[29] O. Madelung (Ed.), Semiconductors—Basic Data, Springer, Berlin, 1996.
[30] J. Partyka, P. Węgierek, P. Żukowski, Yu. Sidorenko, Yu. Szostak, Nucl. Instr. and Meth. B 197 (2002) 60.
[31] N.A. Poklonski, S.A. Vyrko, A.G. Zabrodskii, Semiconductors 41 (2007) 1300.
[32] S. Agarwal, Y.N. Mohapatra, V.A. Singh, J. Appl. Phys. 77 (1995) 3155.
[33] P.K. Giri, Y.N. Mohapatra, Phys. Rev. B 62 (2000) 2497.
[34] P.K. Giri, Y.N. Mohapatra, Mater. Sci. Eng. B 71 (2000) 327.
[35] J. Krynicki, M. Toulemonde, J.C. Muller, P. Siffert, Mater. Sci. Eng. B 2 (1989) 105.
[36] P. Mary, P. Bogdanski, G. Nouet, M. Toulemonde, Appl. Surf. Sci. 43 (1989) 102.
[37] P.K. Giri, Physica B 340–342 (2003) 729.
[38] J. Staňo, V.A. Skuratov, M. Žiška, P. Kováč, Vacuum 78 (2005) 627.